Revista Brasileira de Ciência do Solo

Division – Soil in Space and Time | Commission – Soil Genesis and Morphology

Pedogenesis of pelitic rocks of the Serra da Saudade Formation - Bambuí Group

Luiz Aníbal da Silva Filho[(1)*] (iD), **João Carlos Ker**[(2)] (iD), **Danilo de Lima Camêlo**[(1)] (iD), **Maurício Paulo Ferreira Fontes**[(2)] (iD), **Marcelo Metri Corrêa**[(3)] (iD) **and David Lukas de Arruda Silva**[(2)] (iD)

[(1)] Universidade Federal do Espírito Santo, Departamento de Agronomia, Alegre, Espírito Santo, Brasil.
[(2)] Universidade Federal de Viçosa, Departamento de Solos, Viçosa, Minas Gerais, Brasil.
[(3)] Universidade Federal do Agreste de Pernambuco, Garanhuns, Pernambuco, Brasil.

ABSTRACT: Serra da Saudade Formation corresponds to the upper part of the stratigraphic column of the Bambuí Group. Few studies have addressed the soil properties and pedogenesis of the pelitic rocks rich in potassium minerals of this formation. This study analyzed siltstone-derived soils, some of which are glauconitic (green siltstone; "verdete"), to understand the role of the main pedogenetic factors and processes in the landscape of the Central-West region of the Minas Gerais State, covered by Cerrado vegetation. Nine soil profiles were described, and their morphological, physical, chemical and mineralogical properties were analyzed. Soils were classified as *Neossolos Litólicos* (P1, P3, P6, P8 and P9), *Cambissolos Háplicos* (P2 and P5), *Argissolo Vermelho-Amarelo* (P4) and *Argissolo Acinzentado* (P7). The main active pedogenetic processes identified in the study area are melanization, goethization, argiluviation and elutriation. These are essentially controlled by the nature of the parent material and position of the soil in the relief. Soils are typically shallow, dystrophic, highly Al-saturated and contain essentially quartz and micas in the coarse fractions (sand and silt) and illite/glauconite and kaolinite in the clay fraction. In soil environments with siltstone and green siltstone under "dry forests", the soil water pH was higher and high levels of exchangeable calcium and magnesium, a eutrophic character and high-activity clay were observed. Barium, chromium, lead and zinc contents were high in all studied soils. Green siltstone-derived soils have peculiar physical and chemical properties, divergent from those developed from other glauconitic rocks on the Earth surface. However, greenish tones in horizons are common in all these soils.

Keywords: glauconite, green siltstone, weathering, heavy metal.

INTRODUCTION

Bambuí geological unit consists of siliciclastic and carbonate sedimentary rocks of the Neoproterozoic (>550 million years ago) and lies in the São Francisco Basin, in the central region of Brazil (Uhlein et al., 2019; Silva et al., 2022). It covers part of the states of Minas Gerais, Goiás, Tocantins and Bahia and has a particularly high diversity of pelitic rocks (Lima et al., 2007; Uhlein et al., 2019; Moreira et al., 2021). These rocks gave rise to soils with contrasting characteristics widely used in agriculture (Oliveira et al., 1998; Pereira et al., 2010; Maranhão et al., 2016, 2020).

Soils derived from pelitic rocks are usually fine-textured (silty and/or clayey), yellowish, acidic, dystrophic, and the clay fraction contains essentially muscovite/illite and kaolinite (Barbosa et al., 1991; Pereira et al., 2010). In areas of carbonate or mixed (carbonate-siliciclastic) rocks, the soils have a eutrophic character and high-activity clay (Oliveira et al., 1998; Maranhão et al., 2016, 2020).

Although the pedological pattern is widely acknowledged, pelitic rocks with marked chemical and mineralogical variations can be found in the Bambuí Group (Lima et al., 2007; Moreira et al., 2016, 2020; Uhlein et al., 2019). This calls for studies at different detail levels to deepen the knowledge about soils. One lithostratigraphic unit of the Bambuí Group (Neoproterozoic to Cambrian age) is the Serra da Saudade Formation, which consists of siliciclastic sediments deposited in the epicontinental sea, represented mainly by siltstone, shale, and fine sandstone (Lima et al., 2007; Moreira et al., 2020; Teles et al., 2022).

The most representative display of the Serra da Saudade Formation is found in the homonymous region (Serra da Saudade), between the districts of São Gotardo, Matutina and Cedro do Abaeté, Minas Gerais (Lima et al., 2007; Moreira et al., 2020; Teles et al., 2022). One of the rocks, a dark green siltstone, regionally known as green siltstone, has a particularly high K_2O content (7-14 %), due to the predominance of potassium minerals, e.g., glauconite (40-80 %), K-feldspar (10-15 %), muscovite/illite (5 %) and biotite (2 %) (Moreira et al., 2016). Glauconite accounts for the greenish color of green siltstone and generally has clay-sized particle size (Lima et al., 2007; Moreira et al., 2020). The occurrence of this mineral on the Earth surface is limited, generally to marine-influenced environments (Tedrow, 2002; Andrade et al., 2014, 2018; Skiba et al., 2014; Skoneczna et al., 2019). However, glauconite has been reported in non-marine environments (Huggett and Cuadros, 2010), for example, in hypersaline lakes (Deconinck et al., 1988; Furquim et al., 2010). In the region of Cedro do Abaeté, reworked carbonates (calcirudite and calcarenite) and phosphatic rhythmites (rich in fluorapatite) occur interspersed with green siltstone. The former are thicker and occur frequently in the Serra da Saudade Formation (Lima et al., 2007; Moreira et al., 2020; 2021).

Green siltstone origin is commonly explained by sedimentary and diagenetic processes, such as marine transgression, which favor the formation of glauconite (glauconitization) (Lima et al., 2007; Moreira et al., 2016). Glauconite formation occurs by the dissolution of a precursor clay mineral, most likely illite (the predominant mineral in the sediments) and simultaneous crystallization. This precipitate, resulting from diagenesis in a slightly reducing environment, is transformed into an iron-rich smectite (nontronite), which then undergoes reduction of octahedral Fe^{3+}; Mg^{2+} absorption; selective sorption of K^+ ions from seawater and K^+ fixation in the interlayers, giving rise to glauconite (Odom, 1984; Clauer et al., 1992; Skiba et al., 2014; Moreira et al., 2016). Thus, green siltstone-derived glauconite is an antigenic mineral, formed from illite-rich sediments previously deposited under reducing environmental conditions (Moreira et al., 2016). Another possibility of green siltstone formation in the Serra da Saudade was described by Teles et al. (2022), who suggested that green siltstone is a product of potassium metasomatism in pre-existing detrital sedimentary rocks.

Little is known about the influence of pelitic rocks of the Serra da Saudade Formation on pedogenesis, especially of green siltstone. The characteristics of soils derived from glauconite rocks can be diversified, regardless of the similar environmental conditions during formation (Tedrow, 2002; Skiba et al., 2014; Skoneczna et al., 2019), and the potential for heavy metal contamination may be high (Dooley, 2001; Tedrow, 2002). Summing up, the glauconite content, impurities and rock particle size can significantly influence the properties of the soils formed.

Pedogenetic studies can improve the understanding of the potential and limitations of soils for agricultural and environmental use, as well as for a sustainable management. This study addressed the morphological, physical, chemical and mineralogical properties of soils in areas of pelitic rocks of the Serra da Saudade (Bambuí Group). In addition, we tried to improve the database required to outline appropriate management and conservation strategies for the local features. The hypothesis was that the parent material determines the genesis of soils with divergent characteristics, especially in terms of chemical properties and mineralogical constitution of the clay fraction.

MATERIALS AND METHODS

The study area is part of the Serra da Saudade, in the Central-Western state of Minas Gerais, Brazil (Figure 1a). According to Köppen's classification system, the regional climate is tropical with dry winters (Aw) (Alvares et al., 2013), with annual averages of 1,240 mm rainfall and 23 °C. The vegetation is typical of the Cerrado biome, characterized by forested, savannah-like phytophysiognomies (Ribeiro and Walter, 2008). Geomorphologically, at elevations between 570 and 1,100 m a.s.l., the relief is predominantly mountainous (Figure 1b). The lithology consists of siltstone of the Serra da Saudade Formation (Bambuí Group), which contains basically micas (glauconite, muscovite, biotite and illite), quartz, K-feldspar, kaolinite, goethite and titanium and manganese oxides (Lima et al., 2007; Moreira et al., 2016, 2021).

Based on field observations, nine representative soil profiles of the Serra da Saudade were selected; five were derived from non-glauconitic siltstone (P1, P2, P3, P4 and P5) and four from green siltstone (P6, P7, P8 and P9) (Figures 1c and 2). Non-glauconitic siltstone is generally dark gray or light brown, locally intercalated with calciferous intercalations. It consists mainly of quartz, feldspar and muscovite, whereas glauconite was not detected in the composition (Moreira et al., 2021).

Soils P1, P4, P5, P7 and P9 were covered by typical thin Cerrado vegetation and P2, P3, P6 and P8 by tropical deciduous forest ("dry forest"). Soil horizons were described and sampled as proposed by Santos et al. (2015); the material was air-dried, crumbled and sieved (<2 mm) to obtain air-dried fine earth fraction (ADFE) for physical, chemical and mineralogical analyses. Soils were classified based on the Brazilian Soil Classification System (Santos et al., 2018) and Keys to Soil Taxonomy (Soil Survey Staff, 2014).

Physical and chemical analyses of ADFE samples were carried out, as proposed by Teixeira et al. (2017). The following physical properties were measured: particle-size composition, by ADFE dispersion with 0.1 mol L^{-1} NaOH and vertical mechanical vibration (16 h at 50 rpm); sand content by sieving, and silt and clay contents by the pipette method; clay dispersed in water with the pipette method; particle density using the volumetric flask method. Chemical analyses determined: pH in H$_2$O and in solution with 1 mol L^{-1} KCl (1:2.5 v/v); extraction of exchangeable cations (Ca^{2+}, Mg^{2+} and Al^{3+}) with 1 mol L^{-1} KCl solution, while Ca^{2+} and Mg^{2+} were determined by atomic absorption spectrometry and Al^{3+} by titration with 0.025 mol L^{-1} NaOH; Na, K and P extracted by Mehlich-1 solution, and Na and K were determined by flame photometry, while P by colorimetry; potential acidity (H+Al) by extraction with 0.5 mol L^{-1} calcium acetate solution and determined by titration with 0.025 mol L^{-1} NaOH; total organic carbon (TOC) via wet oxidation with
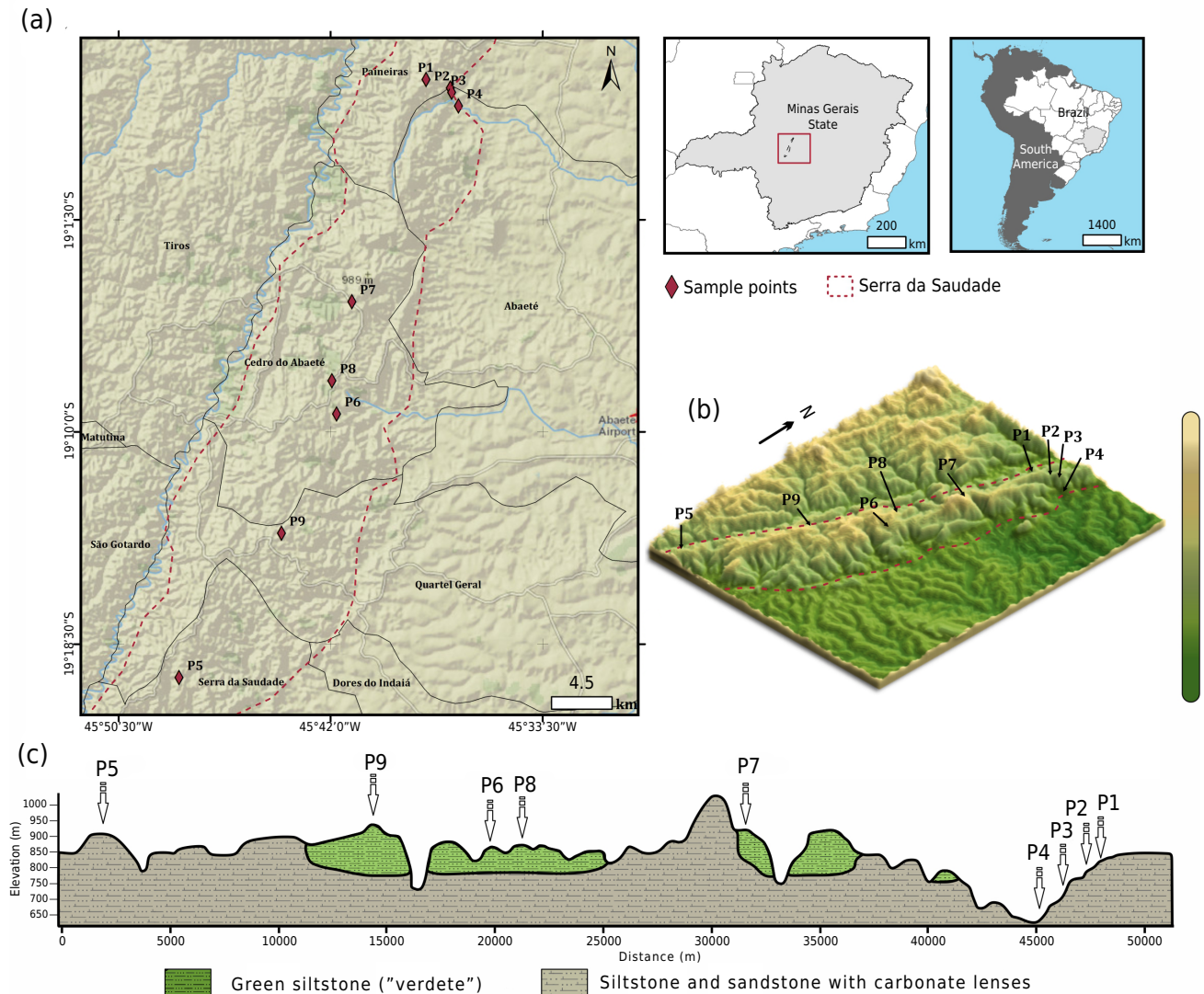
Figure 1. Location of the study area in the central region of Minas Gerais, Brazil (a), distribution of sampled soil profiles in the relief (b) and on the pelitic rocks of the Serra da Saudade Formation, Bambuí Group (c).

0.167 mol L^{-1} K$_2$Cr$_2$O$_7$. The silt/clay ratio, flocculation degree, ΔpH, sum of bases, cation exchange capacity at pH 7.0, base saturation, Al saturation and activity of the clay fraction were calculated (Teixeira et al., 2017; Santos et al., 2018).

Iron was removed from the clay fraction by three successive extractions with sodium citrate-bicarbonate-dithionite (CBD) at 60 °C (Mehra and Jackson, 1960), a single extraction with ammonium acid oxalate (AAO) at pH 3.0 (McKeague and Day, 1966), and determined by atomic absorption spectrometry.

From the clay fraction of the ADFE samples, Si, Al, Fe, Ti, K and P was extracted by sulfuric digestion (H$_2$SO$_4$ 1:1), and total contents of K, Ba, Cr, Pb, Zn, Cd, Co, Cu, Mn, Mo and Ni by triacid digestion (HNO$_3$ + HF + HClO$_4$) (Teixeira et al., 2017). All elements were quantified by inductively coupled plasma atomic emission spectrometry (ICP-OES; Optima 3300 DV, Perkin Elmer). Contents of Si and Al were determined by sulfur digestion and were expressed in the form of oxides and used to calculate the weathering index Ki (Teixeira et al., 2017).

Sand, silt and clay fractions were separated by dispersion with 0.1 mol L^{-1} NaOH and vertical mechanical vibration (16 h at 50 rpm). Sand fraction was removed by sieving (<53 μm) and the silt and clay fractions were separated by sedimentation based on Stokes' Law (Jackson, 1979). Sand, silt and clay fractions were oven-dried at 45 °C and

Figure 2. Representative soil profiles of non-glauconitic siltstone (P1, P2 and P3) and green siltstone (P6, P8 and P9) in the Serra da Saudade Formation, Minas Gerais, Brazil.

analyzed by X-ray diffraction (XRD) in a Shimadzu 6000 diffractometer, operating under the following conditions: 40 kV CuKα radiation, at 30 mA, using a graphite monochromator to scan 4 to 50 °2θ, at steps of 0.02 °2θ s^{-1}. Sand and silt fractions were deposited on hollowed-out glass slides (powder method) after grinding in an agate mortar and sieving (<0.044 mm; 325 mesh), and the clay fraction was mounted on glass slides by smearing (oriented sample).

Clay samples from selected horizons were deferrified with dithionite-citrate-bicarbonate (CBD) and saturated with K and Mg to improve the identification of 2:1 clay minerals (Harris and White, 2008; Teixeira et al., 2017; Silva et al., 2019). For K saturation, a 50 mL falcon tube was filled with 1.0 g of the sample and 10 mL of 1 mol L^{-1} KCl solution, shaken on a shaking table (2 h at 6 rpm), centrifuged at 3000 rpm for 15 min and the supernatant was discarded; this procedure was repeated twice. Sample was washed with 10 mL of distilled water, centrifuged and the supernatant discarded; this procedure was repeated twice. K-saturated sample was deposited in a muffle furnace on a glass slide (oriented sample) for air-drying at 25 °C and successive heating at 330 and 550 °C for 2 h. The same saturation procedure was applied for Mg saturation, but with 1 mol L^{-1} MgCl$_2$ solution. The Mg-saturated sample was mounted on two glass slides (oriented sample), one of which was placed in a vacuum desiccator in an ethylene-glycol-saturated atmosphere for 15 h.

Statistical analysis was performed with PAST 4 software (Hammer et al., 2001). Principal components (PCA), Ward's cluster method and Pearson's correlation analyses were only applied to the variables that met the assumptions of parametric statistical tests, namely: silt; clay; flocculation clay degree; particle density; content of elements in the sulfuric digestion extract, expressed in the form of oxides (SiO_2, Al_2O_3, Fe_2O_3 and TiO_2); Ki weathering index; Ca, Cr and Zn contents in the triacid digestion extract; and Fe content in the extracts CBD (Fe_d) and AAO (Fe_o).

RESULTS AND DISCUSSION

Morphological and physical properties

The depth of the soil profiles varied from 0.20 (P6) to 1.40 m (P7), and the horizon sequences were identified as A – Cr (P1 and P9), A – R (P3, P6 and P8), A – Bi – C (P2 and P5), A – Bt (P4) and A – Bt – BC (P7) (Table 1). These morphological characteristics indicate a predominance of shallow soils in the study area, given by the horizontal strata of pelitic rocks and steep relief at some locations, which are limiting factors for pedogenetic development (Chagas et al., 1997; Pereira et al., 2010).

Yellowish soil horizons (7.5YR and 10YR) are common where the parent material is Fe-poor (Barbosa et al., 1991; Pereira et al., 2010). If low Fe contents are released by the parent material, goethite tends to be formed (xanthization; goethization), since its solubility product is lower than that of ferrihydrite, the precursor of hematite (Schwertmann and Taylor, 1989). On the other hand, in subsurface horizons of deeper soils (P2 and P4), the good drainage conditions and lower organic matter content favor the occurrence of reddish colors resulting from the presence of hematite (rubefaction), with stronger pigmentation than goethite (Schwertmann and Taylor, 1989; Silva and Vidal-Torrado et al., 1999).

Greenish horizons occur in the soils P6, P7, P8 and P9. This indicates presence of glauconite, the mineral that causes the greenish aspect of green siltstone (Lima et al., 2007). This morphological feature was also observed in soils derived from other glauconitic rocks in other regions of the Earth surface (Skiba et al., 2014; Skoneczna et al., 2019).

Surface horizons of soils under dry forest (P2, P3, P6 and P8) have dark colors and low chroma. Under this type of vegetation, the input, transformation and translocation of organic matter by soil fauna promote humin accumulation, which is the most stable fraction of soil organic matter and closely associated with the mineral fraction and a significant melanization process in horizon A (Silva and Vidal-Torrado et al., 1999; Maranhão et al., 2016; 2020).

In relation to the soil structure, the surface horizons contained predominantly granular aggregates, due to the higher organic carbon contents. A moderate medium or large subangular blocky structure was evident in the soil horizons. The presence of larger and more stable soil structures is generally associated with the alternating effects of wetting and drying cycles of the soil mass. In profiles P2, P3 and P8, the presence of angular blocky structures suggested stronger aggregation in these soils, possibly due to the increased levels of flocculating agents (Ca^{2+} and Mg^{2+}) and the mineralogical nature of the clay fraction (Maranhão et al., 2016; 2020).

Silt and clay fractions were predominant in the soils and together accounted for, on average, 85 % of the particle-size distribution of the horizons (Table 2). Thus, most horizons have silty clay loam, silty loam, clay, clay loam and silty clay textures. Silt and clay abundance in the soils was inherited from the parent material (Pereira et al., 2010; Maranhão et al., 2020) and possibly accounted for the yellowish colors of some soils.

Table 1. Morphological properties of sampled soils in the Serra da Saudade Formation, Minas Gerais, Brazil

Hor.	Layer	Color (Munsell)		Structure[1]	Consistency		
		Dry	Wet		Dry	Moist	Wet
	m						
P1 - Neossolo Litólico Distrófico fragmentário (Lithic Udorthents)							
A	0.00-0.03	10YR 6/4	10YR 4/4	mo, f/m, gr	S	FR	MP-MS
Cr1	0.03-0.15		7.5YR 5/6				
Cr2	0.15-0.40		5Y 5/3				
P2 - Cambissolo Háplico Ta Eutrófico típico (Typic Dystrudepts)							
A1	0.00-0.29	10YR 5/3	10YR 3/3	mo, f/ m, gr; mo, f, sbk	SH	FR	MP-MS
A2	0.29-0.47	10YR 5/4	10YR 3/4	mo, f /m, gr; mo, f, sbk	SH	FR	MP-MS
Bi1	0.47-0.67		7.5YR 3/4	mo, m/co, abk/sbk	HA	FI	VP-VS
Bi2	0.67-0.83		7.5YR 4/6	mo, m/co, abk/sbk	HA	FI	VP-VS
Cr1	0.83-1.03		7.5YR 5/8				
Cr2	1.03-1.30+		7.5YR 5/8				
P3 - Neossolo Litólico Eutrófico fragmentário (Lithic Udorthents)							
A1	0.00-0.13	10YR 5/2	10YR 3/3	mo, f/m, gr; mo, m, sbk	SH	FR	MP-MS
A2	0.13-0.45	10YR 5/4	10YR 3/4	mo, f/m, gr; mo, m, abk/sbk	SH	FR	MP-MS
P4 -Argissolo Vermelho-Amarelo Distrófico abrúptico (Typic Haplustults)							
Ap	0.00-0.20	10YR 4/4	10YR 3/4	mo, f/m, gr; mo, f, sbk	SH	FR	MP-MS
Bt1	0.20-0.60		10YR 4/6	mo, m/co, sbk	HA	FR	VP-VS
Bt2	0.60-0.80+		10YR 4/6	mo, m/co, sbk	HA	FR	VP-VS
P5 - Cambissolo Háplico Tb Distrófico típico (Typic Dystrudepts)							
Ap	0.00-0.15	10YR 5/4	10YR 4/4	mo, f/m, gr; mo, f, sbk	SH	FR	SP-MS
Bi	0.15-0.30		10YR 5/6	mo, f/m, gr; mo, f, sbk	HA	FR	SP-MS
BC	0.30-0.50		10YR 5/6	mo, f/m, sbk	HA	FR	SP-MS
C	0.50-0.70		-				
P6 - Neossolo Litólico Eutrófico fragmentário (Lithic Udorthents)							
Ap	0.00-0.20	10YR 5/2	10YR 3/2	st, f/m, gr	SH	Fr	MP-MS
P7 - Argissolo Acinzentado Distrófico abrúptico (Typic Haplustults)							
A1	0.00-0.14	2.5YR 5/2	10YR 3/2	mo, f/m, gr; mo, f, sbk	SH	FR	MP-MS
A2	0.14-0.35	2.5YR 5/2	10YR 4/2	mo, f/m, gr; mo, f, sbk	SH	FR	MP-MS
Bt	0.52-1.13		5Y 4/3	st, m/co, sbk	HA	FI	MP-MS
BC	1.13-1.40+		Gley 1 5/5G	st, m/co, sbk	VD	FI	MP-MS
P8 - Neossolo Litólico Chernossólico fragmentário (Lithic Udorthents)							
A	0.00-0.40	10YR 5/2	10YR 3/2	mo, f/m, gr; mo, f, abk	SH	FR	MP-MS
P9 - Neossolo Litólico Distrófico fragmentário (Lithic Udorthents)							
Ap	0.00-0.15	10YR 5/4	10YR 4/4	mo, f/m, gr; mo, f, sbk	SH	FR	MP-MS
Cr	0.15-0.30	10YR 5/6	10YR 4/6				

Hor.: horizon; [1] Soil structure type. Gr: granular; abk: angular block; sbk: subangular blocky. Size – f: fine; m: medium; co: coarse; vc: very coarse. Degree of development – mo: moderate; st: strong; Consistency – S: soft; SH: slightly hard; HA: hard; VD: very hard; FR: friable; FI: firm; SP: slightly plastic; MP: moderately plastic; VP: very plastic; MS: moderately sticky; VS: very sticky. (*) Described according to Santos et al. (2015). Soils derived from "verdete": P6, P7, P8 and P9.

Table 2. Physical properties of sampled soils in the Serra da Saudade Formation, Minas Gerais, Brazil

Hor.	Sand	Silt	Clay	Textural class	Silt/Clay	FC	Pd
		g kg⁻¹				%	Mg m⁻³
P1 - Neossolo Litólico Distrófico fragmentário (Lithic Udorthents)							
A	100	570	330	Silty clay loam	1.7	55	2.44
Cr1	120	650	230	Silt loam	2.8	57	2.54
Cr2	210	480	310	Clay loam	1.5	97	2.48
P2 - Cambissolo Háplico Ta Eutrófico típico (Typic Dystrudepts)							
A1	70	540	390	Silty clay loam	1.4	67	2.44
A2	50	590	360	Silty clay loam	1.6	58	2.43
Bi1	90	360	550	Clay	0.7	56	2.44
Bi2	40	530	430	Silty clay	1.2	35	2.44
Cr1	80	540	380	Silty clay loam	1.4	47	2.53
Cr2	90	550	360	Silty clay loam	1.5	56	2.56
P3 - Neossolo Litólico Eutrófico fragmentário (Lithic Udorthents)							
A1	160	400	440	Silty clay	0.9	73	2.44
A2	130	520	350	Silty clay loam	1.5	54	2.59
P4 - Argissolo Vermelho-Amarelo Distrófico abrúptico (Typic Haplustults)							
Ap	90	410	500	Silty clay	0.8	80	2.52
Bt1	30	270	700	Clay	0.4	67	2.52
Bt2	30	170	800	Clay	0.2	69	2.50
P5 - Cambissolo Háplico Tb Distrófico típico (Typic Dystrudepts)							
Ap	310	330	360	Clay loam	0.9	69	2.56
Bi	260	380	360	Clay loam	1.1	61	2.63
BC	400	350	250	Loam	1.4	68	2.44
C	420	420	160	Loam	2.6	94	2.60
P6 - Neossolo Litólico Eutrófico fragmentário (Lithic Udorthents)							
Ap	290	290	420	Clay	0.7	64	2.56
P7 - Argissolo Acinzentado Distrófico abrúptico (Typic Haplustults)							
A1	130	340	530	Clay	0.6	55	2.60
A2	170	320	510	Clay	0.6	57	2.57
Bt	80	190	730	Clay	0.3	66	2.60
BC	30	230	740	Clay	0.3	65	2.54
P8 - Neossolo Litólico Chernossólico fragmentário (Lithic Udorthents)							
A	220	260	520	Clay	0.5	67	2.55
P9 - Neossolo Litólico Distrófico fragmentário (Lithic Udorthents)							
Ap	90	470	440	Silty clay	1.1	50	2.40
Cr	150	570	280	Silty clay loam	2.0	50	2.50

Hor.: horizon; FC: flocculated clay degree = (total clay – natural clay) × 100/total clay; Pd: particle density. Soils derived from "verdete": P6, P7, P8 and P9.

In P4 and P7, the clay content increased greatly from horizon A to B, sufficient to characterize an abrupt textural change (Santos et al., 2018). Based on field observations, the textural horizon (Bt) is most likely the product of combined argilluviation and elutriation processes (Vidal-Torrado et al., 2006).

Silt/clay ratio above 0.6 in most soils indicated a low weathering degree (Santos et al., 2018). In the case of P4 and P7, the low silt/clay ratio (≤0.4) in the subsurface horizons was consistent with an intensified pedogenetic development.

Table 3. Chemical properties of sampled soils in the Serra da Saudade Formation, Minas Gerais, Brazil

Hor.	pH(1:2.5)			Ca^{2+}	Mg^{2+}	K^+	Na^+	Al^{3+}	H+Al	SB	CEC_T	CEC_R	V	m	P	TOC
	H_2O	KCl	ΔpH													
				— cmol$_c$ kg^{-1} —									%		mg kg^{-1}	g kg^{-1}
P1 - *Neossolo Litólico Distrófico fragmentário* (Lithic Udorthents)																
A	5.06	3.95	-1.1	0.2	0.2	0.1	0.0	2.5	4.3	0.6	4.8	14.6	11	82	1	6
Cr1	5.16	4.02	-1.1	0.1	0.1	0.1	0.0	2.9	4.4	0.2	4.6	20.1	5	93	1	3
Cr2	5.44	4.09	-1.3	0.0	0.2	0.1	0.0	3.1	4.4	0.3	4.7	15.1	6	92	1	2
P2 - *Cambissolo Háplico Ta Eutrófico típico* (Typic Dystrudepts)																
A1	5.42	4.37	-1.1	9.7	1.3	0.1	0.0	0.0	7.5	11.1	18.6	47.8	60	0	2	13
A2	5.69	4.55	-1.1	9.2	1.0	0.1	0.0	0.0	7.4	10.3	17.7	49.1	58	0	1	12
Bi1	5.97	4.69	-1.3	9.0	1.5	0.1	0.0	0.0	6.8	10.6	17.4	31.6	61	0	2	6
Bi2	5.88	4.75	-1.1	7.4	1.3	0.1	0.1	0.0	6.4	8.9	15.3	35.5	58	0	3	4
Cr1	5.67	4.42	-1.3	8.6	1.9	0.1	0.1	0.0	6.0	10.7	16.6	43.8	64	0	3	2
Cr2	6.08	4.82	-1.3	7.4	2.4	0.1	0.1	0.0	5.5	10.0	15.4	42.9	64	0	2	1
P3 - *Neossolo Litólico Eutrófico fragmentário* (Lithic Udorthents)																
A1	6.34	5.11	-1.2	5.5	3.1	0.5	0.0	0.0	7.4	9.1	16.5	37.4	55	0	4	14
A2	5.79	4.32	-1.5	5.6	1.1	0.2	0.0	0.0	6.8	6.9	13.7	39.2	50	0	1	5
P4 - *Argissolo Vermelho-Amarelo Distrófico abrúptico* (Typic Haplustults)																
Ap	5.10	3.81	-1.3	1.6	0.2	0.0	0.0	1.6	4.7	1.9	6.6	13.2	29	45	3	16
Bt1	5.19	3.77	-1.4	2.8	0.4	0.0	0.0	2.6	4.1	3.2	7.3	10.4	44	45	2	11
Bt2	5.02	3.75	-1.3	2.0	0.5	0.0	0.0	3.0	3.3	2.5	5.8	7.2	44	54	1	8
P5 - *Cambissolo Háplico Tb Distrófico típico* (Typic Dystrudepts)																
Ap	4.84	3.89	-1.0	0.3	0.3	0.1	0.0	2.8	5.0	0.8	5.8	16.1	13	79	1	16
Bi	4.90	3.94	-1.0	0.1	0.1	0.0	0.0	2.4	5.2	0.2	5.4	14.9	4	92	1	12
BC	4.69	4.11	-0.6	0.0	0.0	0.0	0.0	2.3	4.0	0.1	4.1	16.5	3	95	1	7
C	5.26	4.26	-1.0	0.0	0.0	0.0	0.0	1.9	3.2	0.1	3.3	20.4	3	95	1	3
P6 - *Neossolo Litólico Eutrófico fragmentário* (Lithic Udorthents)																
Ap	6.04	4.87	-1.2	5.5	1.4	0.4	0.0	0.0	6.0	7.3	13.3	31.6	55	0	4	18
P7 - *Argissolo Acinzentado Distrófico abrúptico* (Typic Haplustults)																
A1	5.11	3.90	-1.2	2.6	1.1	0.2	0.0	1.6	4.5	3.9	8.4	15.9	47	28	5	16
A2	5.04	3.88	-1.2	2.4	0.4	0.1	0.0	1.9	3.9	3.0	6.8	13.4	43	39	5	12
Bt	5.11	3.88	-1.2	0.8	0.1	0.1	0.0	2.0	3.2	1.0	4.2	5.7	24	66	2	5
BC	5.05	3.82	-1.2	0.5	0.2	0.1	0.0	2.9	4.2	0.7	4.9	6.6	14	81	1	5
P8 - *Neossolo Litólico Chernossólico fragmentário* (Lithic Udorthents)																
A	6.33	5.46	-0.9	9.9	3.1	0.7	0.0	0.0	6.2	13.8	20.0	38.4	69	0	6	16
P9 - *Neossolo Litólico Distrófico fragmentário* (Lithic Udorthents)																
Ap	5.10	3.97	-1.1	0.3	0.4	0.1	0.0	2.1	5.9	0.8	6.7	15.1	12	73	4	15
Cr	5.66	4.09	-1.6	0.2	0.0	0.1	0.0	1.8	3.6	0.3	3.9	13.9	9	84	1	6

Hor.: horizon; ΔpH: pH_{KCl} – pH_{H2O}; SB: sum of base; CEC_T: total cation exchange capacity (SB + H+Al); CEC_R: clay activity ($CTC_R = CEC_T \times 1000$/ total clay); V: saturation of bases ($V = SB \times 100/CEC_T$); m: saturation of aluminum [$m = (100 \times Al^{3+})/(SB + Al^{3+})$]; P: phosphorus extracted by Mehlich-1; TOC: total organic carbon. Soils derived from "verdete": P6, P7, P8 and P9.

In almost all horizons, the flocculation clay degree (FD) was below 70 %. Clay dispersion phenomenon in soils is mainly favored by low levels of organic matter and Fe oxyhydroxides, which are cementing agents with a high specific surface area (Donagemma et al., 2003; Almeida Neto et al., 2009). According to these authors, the positive surface charges of Fe oxyhydroxides are expected to interact strongly with kaolinite, by charge neutralization, making the formation of more stable aggregates possible. Clay dispersion can be favored by 2:1 clay minerals (Corrêa et al., 2003), which are components that increase the negative charge density, favoring clay dispersion in water.

Chemical properties

Soils differed markedly in terms of chemical properties (Table 3). Soil reaction classes ranged from strongly acidic (pH_{H2O}: 4.3 – 5.3) to moderately acidic (pH_{H2O}: 5.4 – 6.5) (Santos et al., 2018). In P2, P3, P6 and P8, pH_{H2O} values around 5.6 caused precipitation of the aluminum ion, resulting in zero values of Al^{3+} and Al saturation (m%). Negative ΔpH values indicate predominance of cation exchange capacity in soils.

Soils P2, P3, P6 and P8 were characterized as eutrophic, with base saturation of more than 50 %. The Ca^{2+} predominated in the soil sorptive complex (5.5 - 9.9 $cmol_c$ kg^{-1}), followed by Mg^{2+} (1.0 - 3.1 $cmol_c$ kg^{-1}). These soils had the highest CEC_T values (13.3 - 20.0 $cmol_c$ kg^{-1}) and high soil activity clay (CEC_R >27 $cmol_c$ kg^{-1}). These chemical characteristics suggested a contribution of carbonates to soil formation (Lima et al., 2007; Moreira et al., 2016, 2021). In fact, P2, P3, P6 and P8 lie in areas with dry forest vegetation, which indicates the occurrence of rocks influenced by carbonates in the Bambuí Group (Maranhão et al., 2016; 2020). These components (carbonates) of the parent material, at a location with limited base leaching, trigger the genesis of eutrophic soils, the main environmental condition for the establishment of dry forest vegetation (Ribeiro and Walter, 2008).

The possibility of the participation of phosphates in increasing the chemical fertility of siltstone-derived soils of the Serra da Saudade Formation was mentioned by Lima et al. (2007). However, in view of the low P contents (≤ 6 mg kg^{-1}) of the studied soils, this possibility was ruled out.

Most soils (P1, P4, P5, P7 and P9) are highly acidic, dystrophic and highly Al-saturated (m%). These characteristics are frequently reported for soils derived from rocks of the Bambuí Group, uninfluenced by carbonates (Barbosa et al., 1991; Pereira et al., 2010).

The Ki index ranged from 2.10 to 4.23, and was highest in soils derived from green siltstone (P6, P7, P8 and P9) (Table 4). These values indicate a low weathering degree and limited silica removal from soils. The high Ki values in green-siltstone-derived soils (Ki ≥ 3.37), especially in P6 and P8, suggested a considerable participation of 2:1 clay minerals in the clay composition (Mota et al., 2007). This can be explained by the proximity of the underlying rock, which limits water percolation and, consequently, desilication (Pinheiro Junior et al., 2021), as well as the abundance of these clay minerals in green siltstone (Lima et al., 2007; Moreira et al., 2016). The Fe_2O_3 and TiO_2 contents were considered low, as also reported by Pereira et al. (2010) and Maranhão et al. (2016; 2020) for soils of the Bambuí Group.

The Fe_d values were low, and the lowest found in soils derived from green siltstone. This indicated a slow release of Fe from primary minerals, which reduces Fe precipitation in the form of crystalline Fe oxyhydroxides (Skiba et al., 2014; Pinheiro Junior et al., 2021). The lowest Fe_d in P6, P8 and P9 could be explained by the imperfect drainage conditions caused by the lithic contact, which induced Fe reduction and leaching (Maranhão et al., 2020).

The low Fe_o/Fe_d ratio indicated a predominance of crystalline forms of Fe oxyhydroxides. The higher Fe_o/Fe_d ratio in the upper horizons was associated with a higher organic matter content, responsible for Fe complexation and, consequently, reduced crystallinity of Fe oxyhydroxides and increased Fe_o concentration (Schwertmann and Taylor, 1989; Maranhão et al., 2020).

The Fe_d/Fe_s ratio was lower (≤ 0.24) in soils derived from green siltstone (P6, P7, P8 and P9) than in the other soils (>0.45). This result and the high Pearson correlation between SiO_2 and Fe_2O_3 (r = 0.9123; p<0.01; n = 8), identified in P6, P7, P8 and P9, suggested that green siltstone gave rise to soils with a significant concentration of secondary Fe-bearing mineral. In fact, glauconite [K_2(Mg Fe)$_2Al_6$(Si_4O_{10})$_3$(OH)$_{12}$] is an iron-rich dioctahedral mica

in the crystalline structure (especially of Fe^{3+}) (Odom, 1984; Rieder et al., 1998), abundant in green siltstone (Lima et al., 2007; Moreira et al., 2016), and tends to constitute the clay fraction of the soil (Skiba et al., 2014; Skoneczna et al., 2019).

Potassium contents determined by sulfuric (K_s) and triacid (K_t) digestion resulted in K_s/K_t ratios close to 1 in most soils (Table 5), indicating that the clay fraction is the main source of this element. Soils P6, P7, P8 and P9 had the highest K_t contents, in line with the chemical and mineralogical composition of green siltstone (Lima et al., 2007; Moreira et al., 2016).

Table 4. Silicon, Al, Fe and Ti extracted by sulfur digestion (expressed in the form of oxides), molecular relationship Ki, selective dissolution of Fe (Fe_d and Fe_o) and their relationships

Hor.	SiO_2	Al_2O_3	Fe_2O_3	TiO_2	Ki	Fe_d	Fe_o	Fe_o/Fe_d	Fe_d/Fe_s
			g kg⁻¹				g kg⁻¹		
P1 - Neossolo Litólico Distrófico fragmentário (Lithic Udorthents)									
A	175.3	106.6	67.0	1.7	2.80	37	5	0.13	0.79
Cr1	215.1	130.4	58.5	2.1	2.80	21	4	0.18	0.51
Cr2	224.8	136.8	88.9	2.9	2.79	36	5	0.14	0.58
P2 - Cambissolo Háplico Ta Eutrófico típico (Typic Dystrudepts)									
A1	160.2	121.9	59.1	2.2	2.23	19	10	0.51	0.46
A2	126.6	89.2	47.2	2.2	2.41	20	9	0.43	0.61
Bi1	181.2	120.6	59.7	3.1	2.56	28	6	0.21	0.66
Bi2	174.5	141.3	67.7	2.8	2.10	38	5	0.14	0.80
Cr1	225.2	145.3	72.4	2.7	2.64	39	5	0.13	0.76
Cr2	183.8	77.6	39.6	1.4	4.03	24	4	0.16	0.87
P3 - Neossolo Litólico Eutrófico fragmentário (Lithic Udorthents)									
A1	173.8	103.7	60.7	2.5	2.85	12	7	0.57	0.28
A2	155.4	105.3	84.1	1.8	2.51	32	5	0.16	0.55
P4 - Argissolo Vermelho-Amarelo Distrófico abrúptico (Typic Haplustults)									
Ap	113.4	78.8	37.1	1.8	2.45	16	10	0.64	0.61
Bt1	167.8	112.5	49.9	2.6	2.54	18	6	0.34	0.51
Bt2	211.8	158.9	74.0	2.4	2.27	24	4	0.17	0.45
P5 - Cambissolo Háplico Tb Distrófico típico (Typic Dystrudepts)									
Ap	161.4	113.5	49.5	1.6	2.42	20	8	0.41	0.59
Bi	180.7	121.0	53.0	1.8	2.54	30	7	0.24	0.81
BC	169.8	111.6	45.7	1.4	2.59	20	4	0.21	0.61
C	159.3	120.1	44.5	1.4	2.26	28	3	0.10	0.91
P6 - Neossolo Litólico Eutrófico fragmentário (Lithic Udorthents)									
Ap	250.5	103.8	69.3	2.4	4.10	2	2	1.00	0.01
P7 - Argissolo Acinzentado Distrófico abrúptico (Typic Haplustults)									
A1	210.6	92.3	52.1	2.4	3.88	2	2	0.82	0.05
A2	210.2	102.3	59.6	3.3	3.49	6	2	0.33	0.15
Bt	273.3	133.2	70.4	3.4	3.49	12	2	0.14	0.24
BC	306.0	149.8	78.0	3.0	3.47	8	1	0.12	0.14
P8 - Neossolo Litólico Chernossólico fragmentário (Lithic Udorthents)									
A	244.5	98.3	61.3	1.7	4.23	1	1	1.00	0.01
P9 - Neossolo Litólico Distrófico fragmentário (Lithic Udorthents)									
Ap	230.9	99.2	53.6	3.1	3.96	1	1	0.63	0.03
Cr	270.5	136.3	68.4	2.8	3.37	2	1	0.31	0.05

Ki = (SiO_2/Al_2O_3) × 1.7 (Teixeira et al., 2017); Fes = Fe_2O_3 / 1.43. Soils derived from "verdete": P6, P7, P8 and P9.

Table 5. Potassium content extracted by sulfuric (Ks) and triacid (Kt) digestion, Ks/Kt, ratio and heavy metal contents

Hor.	K_s	K_T	K_s/K_T	Ba	Cr	Pb	Zn
	——— g kg^{-1} ———			——— mg kg^{-1} ———			
P1 - *Neossolo Litólico Distrófico fragmentário* (Lithic Udorthents)							
A	19.2	24.9	0.8	336.7	77.6	9.3	31.5
Cr1	22.2	29.3	0.8	368.6	96.7	10.5	58.7
Cr2	29.0	34.9	0.8	434.3	99.8	37.3	39.9
P2 - *Cambissolo Háplico Ta Eutrófico típico* (Typic Dystrudepts)							
A1	14.7	14.3	1.0	264.6	61.1	16.3	59.9
A2	11.0	14.4	0.8	253.6	62.2	24.3	80.8
Bi1	14.3	15.2	0.9	247.3	71.7	13.2	27.6
Bi2	16.1	19.5	0.8	307.5	85.5	18.6	38.7
Cr1	18.8	22.9	0.8	341.1	96.2	15.4	69.6
Cr2	9.3	19.2	0.5	276.9	79.9	4.5	56.5
P3 - *Neossolo Litólico Eutrófico fragmentário* (Lithic Udorthents)							
A1	15.4	19.2	0.8	300.0	85.7	14.7	50.7
A2	14.2	19.7	0.7	310.2	108.4	22.5	35.1
P4 - *Argissolo Vermelho-Amarelo Distrófico abrúptico* (Typic Haplustults)							
Ap	8.2	11.2	0.7	187.4	67.8	0.0	0.0
Bt1	10.4	13.2	0.8	225.3	73.6	7.3	0.0
Bt2	13.5	15.8	0.9	250.4	90.1	7.6	0.0
P5 - *Cambissolo Háplico Tb Distrófico típico* (Typic Dystrudepts)							
Ap	11.9	14.5	0.8	261.5	65.2	8.0	30.6
Bi	12.9	13.7	0.9	290.0	58.2	5.9	0.0
BC	12.5	14.0	0.9	201.6	56.9	6.5	0.0
C	13.3	19.1	0.7	327.3	56.4	11.7	2.3
P6 - *Neossolo Litólico Eutrófico fragmentário* (Lithic Udorthents)							
Ap	34.5	42.2	0.8	311.0	110.1	12.4	125.7
P7 - *Argissolo Acinzentado Distrófico abrúptico* (Typic Haplustults)							
A1	21.6	30.3	0.7	458.1	90.4	9.4	35.0
A2	24.7	34.4	0.7	486.0	91.8	9.4	40.2
Bt	27.4	33.9	0.8	462.2	120.7	12.9	6.0
BC	32.2	39.9	0.8	502.5	91.0	12.3	39.4
P8 - *Neossolo Litólico Chernossólico fragmentário* (Lithic Udorthents)							
A	30.1	51.4	0.6	566.7	89.7	5.9	98.4
P9 - *Neossolo Litólico Distrófico fragmentário* (Lithic Udorthents)							
Ap	27.2	44.2	0.6	439.4	89.9	0.8	43.2
Cr	33.5	50.2	0.7	563.2	96.3	21.9	85.2

Levels of Cd, Co, Cu, Mn, Mo and Ni were below the equipment detection limit. Soils derived from verdete: P6, P7, P8 and P9.

The wide range of heavy metal contents in the soils was noteworthy: Ba (187.4 - 566.7 mg kg^{-1}); Cr (56.4 - 120.7 mg kg^{-1}); Pb (0 - 37.3 mg kg^{-1}) and Zn (0 - 125.7 mg kg^{-1}) (Table 5). These levels exceeded the threshold established by the Environmental Policy Council of the state of Minas Gerais for: Ba (>93 mg kg^{-1}), Cr (>75 mg kg^{-1}), Pb (>19.5 mg kg^{-1}) and Zn (>46.5 mg kg^{-1}) (Copam, 2011). Among the heavy metals analyzed, Ba was found at the highest levels, notably in the green-siltstone-derived soils. This element is abundant in areas formed by marine sedimentation, such as the Serra da Saudade Formation (Lima et al., 2007). Barium can be associated with micas, where it substitutes K isomorphically (Liguori et al., 2016). High Ba values were also reported in glauconitic soils in New Jersey (USA) (Dooley, 2001).

These high heavy metal levels (Ba, Cr, Pb, and Zn) in the soils of the Serra da Saudade Formation raise environmental concerns. The elements may be accumulated in plants, posing a health risk to local human consumers (Jalali and Meyari, 2022). Furthermore, green siltstone rock has properties of a potassium fertilizer (Santos et al., 2015; Silva and Lana, 2015), but could cause heavy metal accumulation in soils of other regions over time and could contaminate vegetables in production (Njuguna et al., 2019).

Two groups of soils were identified by principal component (PCA) and clustering analysis, explained mainly by the parent material (Figure 3). The variables with the greatest contribution to group 1 (siltstone-derived soils) were Fe_d, Fe_o, flocculation clay degree (FC) and silt, while for group 2 (green-siltstone-derived soils), these variables were SiO_2, Cr, Ba, particle density (Pd), Ki and Zn. In group 1, the highest silt contents were a legacy of the siliciclastic nature of the parent material (Lima et al., 2007; Moreira et al., 2016), while the highest iron contents associated with Fe oxyhydroxides may be the result of biotite changes or inherited, given the presence of goethite in the parent material (Moreira et al., 2016). In group 2, SiO_2 and Ki indicated the beginning of weathering in the soils, while the higher Cr, Zn and Ba contents were related to glauconitic soils (Dooley, 2001).

Mineralogy of sand, silt and clay

X-ray patterns indicated the presence of quartz in the sand (Figure 4a) and silt (Figure 4b) fractions. Mica and K-feldspar were also detected in the coarse fractions (sand and silt) of all soils but P4. X-ray patterns of the clay fraction of soils derived from non-glauconitic siltstones (Figure 5) and green siltstone (Figure 6) showed very strong diffraction peaks for mica and kaolinite and a weaker peak, attributed to goethite and hematite. Mineralogical composition of the sand, silt and clay fractions reflected the siliciclastic nature of the pelitic rocks of the Serra da Saudade Formation (Lima et al., 2007; Moreira et al., 2016, 2021), which is common in the soils of the Bambuí Group (Oliveira et al., 1998; Pereira et al., 2010; Maranhão et al., 2016, 2020).

For soil P4, a higher weathering degree than that of the other soils was inferred since mica was detected in the clay fraction only, and no K-feldspar was in the coarse fractions. These minerals are common mineralogical components of the parent material (Moreira et al., 2021) and therefore tend to constitute the sand and silt fractions (Pereira et al., 2010).
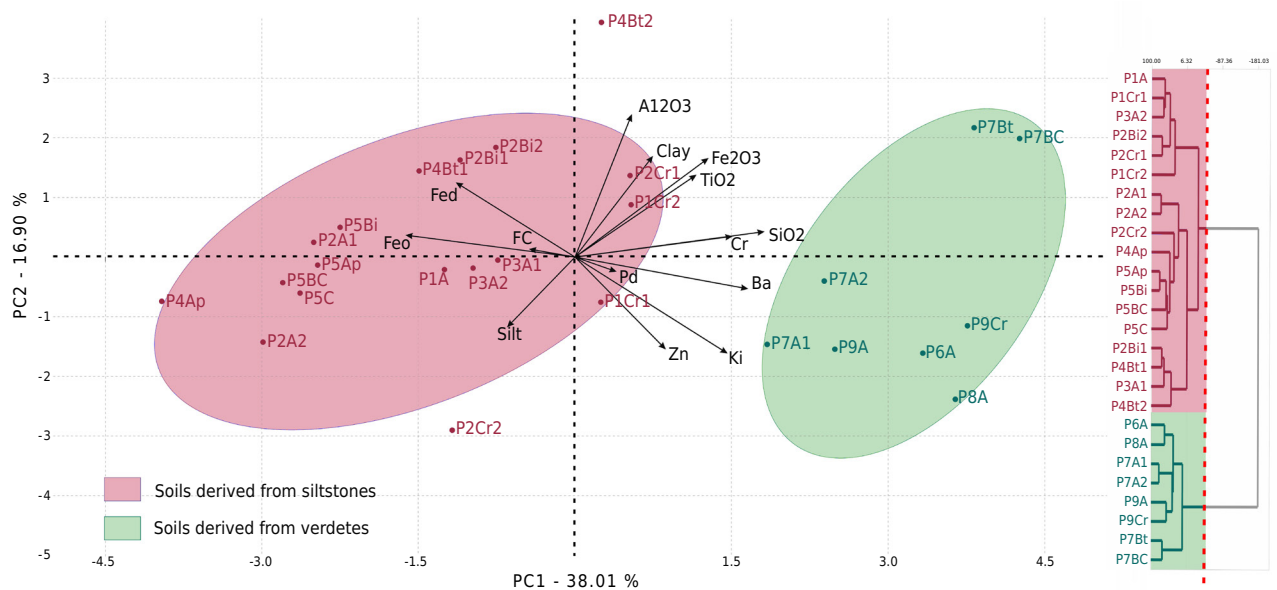

Figure 3. Principal component analysis (PCA) and grouping of the studied soils.
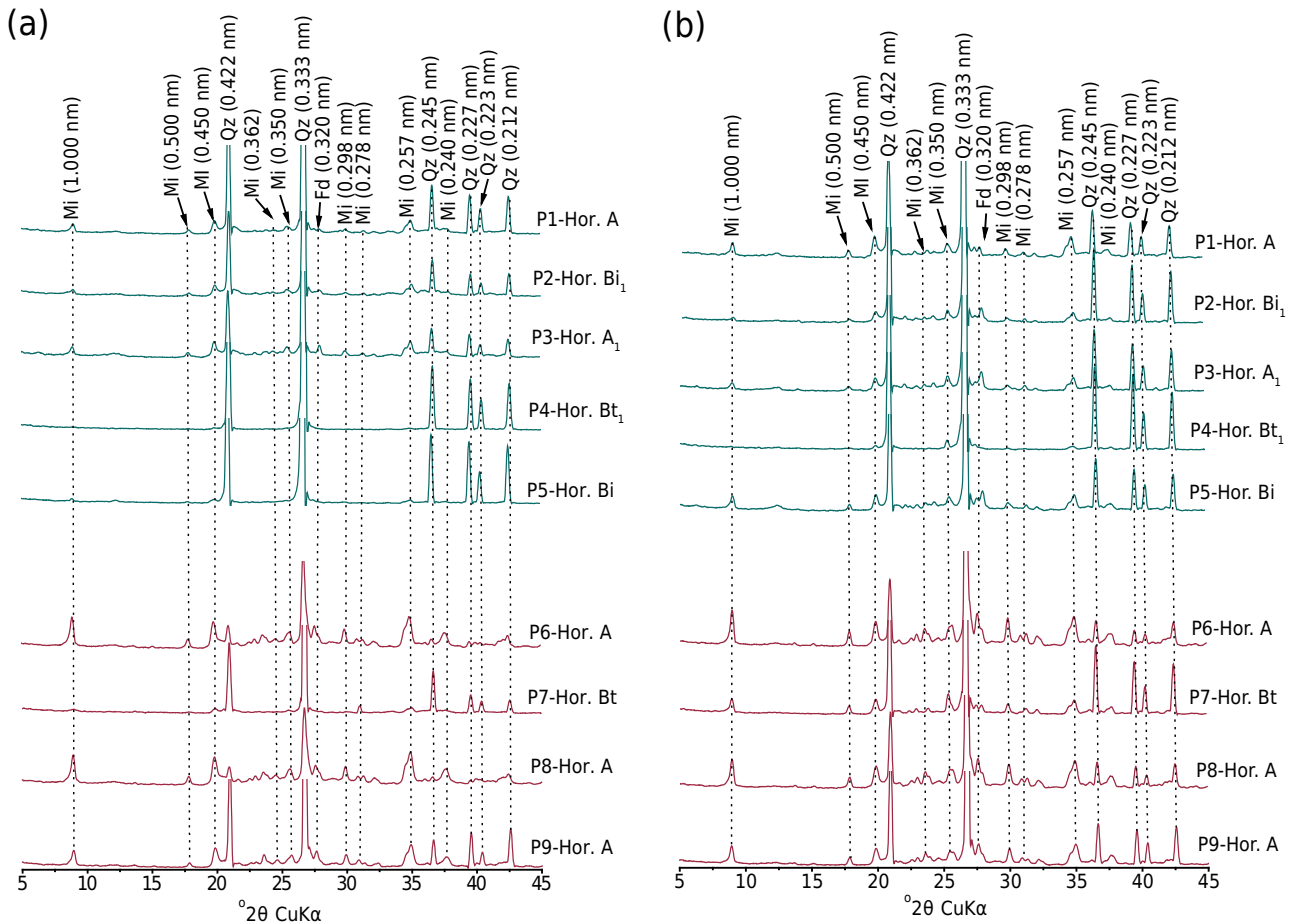
Figure 4. X-ray patterns of sand (a) and silt (b) fractions of selected horizons of soils derived from siltstone (blue lines) and green silstone (red lines), sampled in the Serra da Saudade Formation, Minas Gerais, Brazil. Identified minerals: Mi: mica; Qz: quartz; Fd: K-feldspar. Values in parentheses indicate the distance between adjacent planes, in nanometers (nm).

For P2, P3, P6 and P8, the X-ray patterns had no peaks indicating carbonates. This shows that the carbonate levels were lower than the detection limit of X-ray diffractometry, in agreement with their low levels in the composition of pelitic rocks of the Serra da Saudade Formation (Lima et al., 2007; Moreira et al., 2021).

Micaceous minerals (illite and glauconite) are abundant in the clay fraction of green siltstone -derived soils (P6, P7, P8 and P9). Therefore, the values of the molecular Ki ratio and K contents (K_s and K_t) were higher. Muscovite, illite and glauconite were the main micas identified in pelitic rocks of the Serra da Saudade Formation; glauconite was only found in green siltstone (Lima et al., 2007; Moreira et al., 2016, 2021).

Kaolinite is poorly crystalline, as shown by the broad asymmetric 001 peak, especially in soils derived from green siltstone. This was interpreted as the presence of interstratified kaolinite-mica, suggesting progressive kaolinization in the soils. In this process, the pre-existing mica is not fully dissolved, followed by kaolinite recrystallization, and a topotactic transformation, signaled by an intermediate phase (Andrade et al., 2019). Initially, the 2:1 clay mineral undergoes gradual removal of tetrahedral layers, resulting in a kaolinite layer. In the solid state, modifications of the 2:1 clay mineral continue, such as removal or inversion of Si tetrahedra, replacement of octahedral Mg or Fe by Al, and cation removal (mainly of K) from the layers (Ryan and Huertas, 2009). This is a slow process, which allows the formation of interstratified kaolinite-mica and, subsequently, kaolinite (Andrade et al., 2019). The resulting kaolinite is generally disordered and Fe-rich (Ryan and Huertas, 2009).
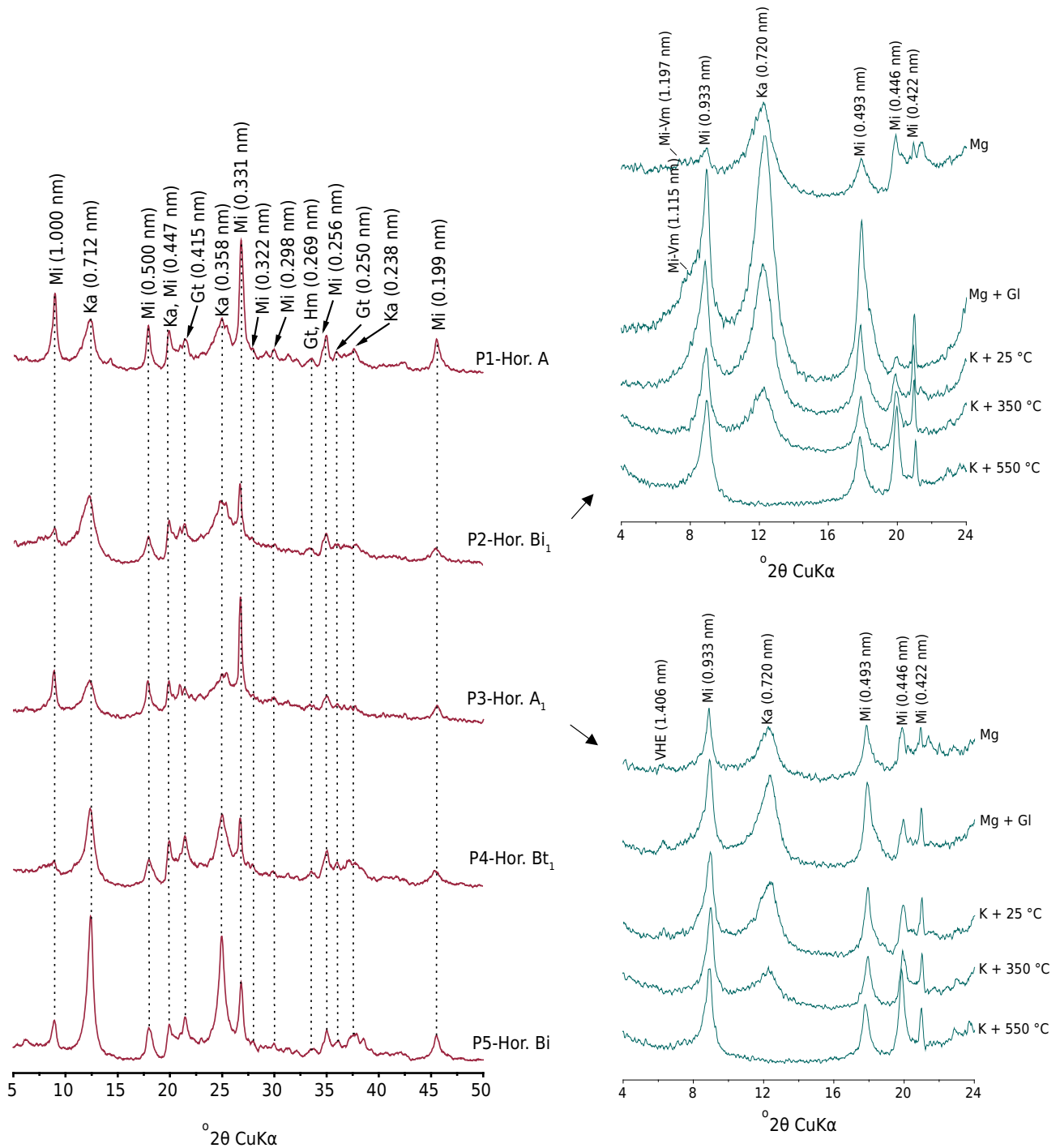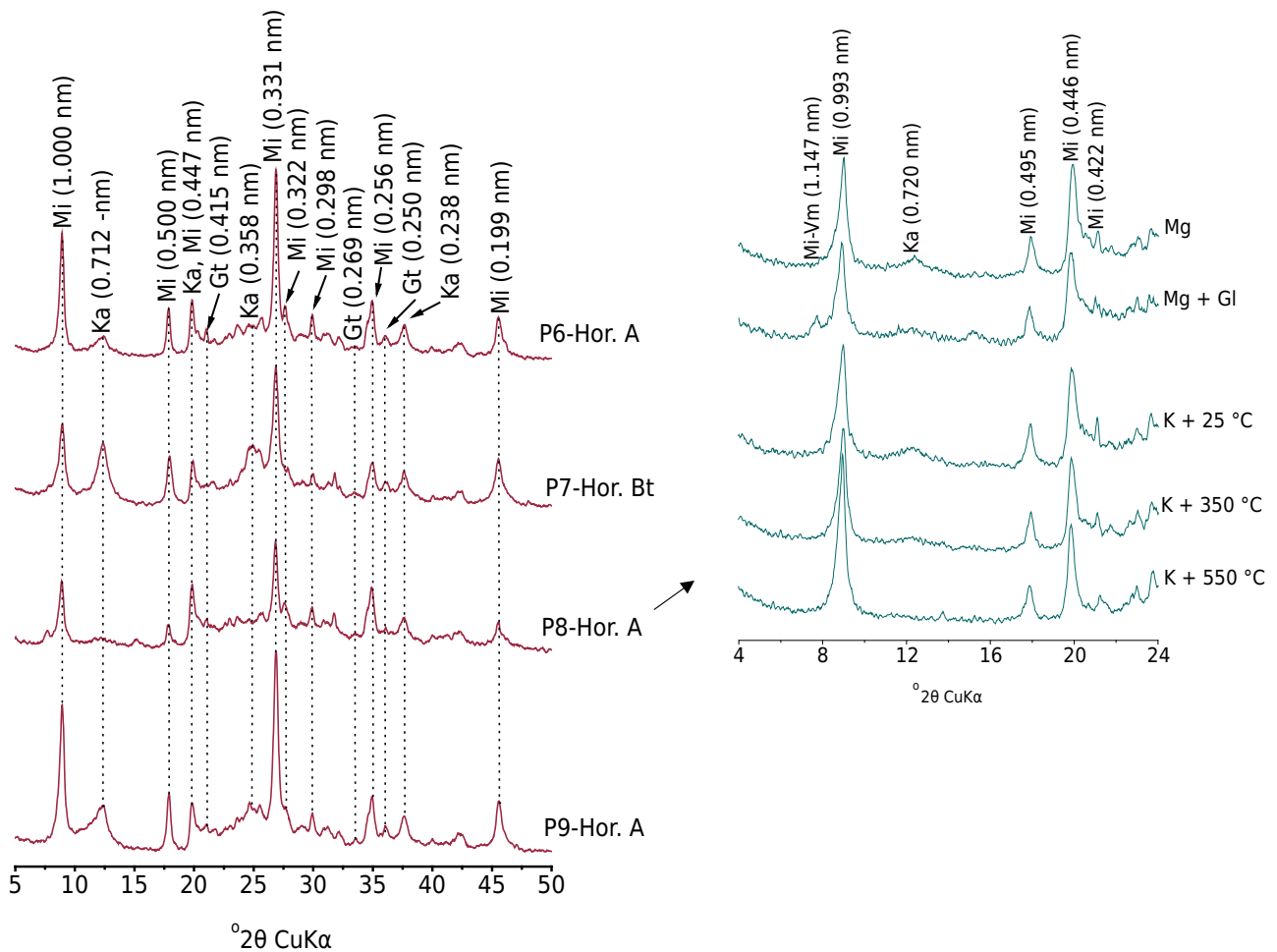
Figure 5. X-ray patterns of the clay fraction of soil horizons sampled in the Serra da Saudade Formation, Minas Gerais, Brazil. Treatments for identification of 2:1 minerals in P3 and P4 are indicated by the dashed arrow. Mi: mica (illite and/or glauconite); Ka: kaolinite; Gt: goethite; Hm: hematite; Vm: vermiculite; VHI: vermiculite with hydroxy-Al interlayers. Values in parentheses indicate the distance between adjacent planes, in nanometers (nm).

X-ray patterns of the clay fraction of P2, P3 and P8 showed a peak at 1.147-1.406 nm, which is characteristic of expansive 2:1 phyllosilicates, as indicated by the high activity values of the clay fraction. Therefore, we applied appropriate treatments to identify these minerals in the samples (Figures 5 and 6). In P2, the peak at 1.197 nm was slightly expanded after solvation with ethylene glycol (Mg + Gl), suggesting the occurrence of interstratified mica-vermiculite. The intensification of the peak at 1.00 nm in the treatment with K saturation and heating at 350 °C reinforced the presence of vermiculite. In profile P3, the persistence of the diffraction peak around 1.406 nm after saturation with Mg and

Figure 6. X-ray patterns of the clay fraction of soil horizons sampled in the Serra da Saudade Formation, Minas Gerais, Brazil. Treatments for identification of 2:1 minerals in P8 are indicated by the dashed arrow. Mi: mica (illite and/or glauconite); Ka: kaolinite; Gt: goethite; Hm: hematite; Vm: vermiculite. Values in parentheses indicate the distance between adjacent planes, in nanometers (nm).

Mg + Gl, as well as its disappearance in K-saturated and heated (350 and 550 °C) samples indicated the presence of vermiculite with hydroxy-Al between layers. In P8, the peak at 1.147 nm was attributed to the interstratified mica-vermiculite phase, considering its persistence after treatment with Mg + Gl. Finally, the disappearance of the d001 peak of kaolinite after the K-saturation treatment and heating at 550 °C indicated the absence of chlorite in P2, P3 and P8.

Mica-vermiculite presence in P2 and P8 indicated that vermiculite is formed in solid state from weathering mica (illite and, or glauconite) (Skiba et al., 2014; Andrade et al., 2019; Skoneczna et al., 2019). This transition from mica to vermiculite is a consequence of intense weathering and apparently occurs concomitantly with the mica-to-kaolinite transition, but in a separate process (Andrade et al., 2019). According to Skiba et al. (2014), the transformation of glauconite into 2:1 expandable clay minerals involved selective leaching of Mg and octahedral Fe and probably a structural reorganization.

The occurrence of vermiculite with hydroxy-Al interlayers (VHI) in P3 indicated better drainage conditions (Georgiadis et al., 2020), owing to the inclined orientation of the layers in the parent material (Figure 2), an unusual characteristic in siltstone of the Serra da Saudade Formation (Lima et al., 2007; Teles et al., 2022). Minerals interlayered with hydroxy-Al can occur under wide-ranging pedoenvironmental conditions (Georgiadis et al., 2020). In profile P3, the interlayered K in micas was replaced by exchangeable hydrated cations due to the influence of weathering. Due to the characteristics of the parent

material, the increased water flow favored the weathering processes, base leaching and, consequently, soil acidification. Low pH promotes Al^{3+} release from silicates (e.g., micas and feldspars) and increases their mobility in the soil solution, facilitating the process of intercalation in expansive 2:1 clay minerals by cation exchange. The Al^{3+} in the interlayers is polymerized and forms minerals with hydroxy-Al interlayers, for example, vermiculite with hydroxy-aluminum interlayers (VHI) (Georgiadis et al., 2020).

Although P1 and P5 had a peak around 1.4 nm, no treatments for 2:1 clay mineral differentiation were applied. As these are acidic, dystrophic and low-activity clay soils, this peak suggested the presence of 2:1 clay mineral with interlayered hydroxy-Al, possibly VHI (Pereira et al., 2010).

CONCLUSION

The studied soils are characterized by a low degree of pedogenetic development and a mineralogical assemblage of basically quartz, micas (muscovite and/or biotite) in the sand and silt fractions, illite/glauconite, kaolinite and goethite in the clay fraction. In pedoenvironments influenced by carbonates from parent material, identified by the typical "dry forest" vegetation, eutrophic soils occur, with high calcium and magnesium contents in the sorptive complex, and the presence of vermiculite, mica-vermiculite or vermiculite with interlayered hydroxy-Al. The main pedogenetic processes identified were melanization, goethization, argilluviation and elutriation.

Soils derived from green siltstone have horizons with greenish tones due to the presence of glauconite, a common characteristic of soils derived from glauconitic rocks in different regions of the Earth surface. Parent materials defined the formation of soils with contrasting characteristics, especially regarding horizon color, chemical fertility, and mineralogical constitution of the clay fraction, confirming the study hypothesis.

Most soils had considerable barium, chromium, lead and zinc contents. Therefore, we suggest evaluating the bioavailability of these heavy metals in future research, which is important for assessing the toxicity risk to organisms, and to establish a regulatory system for land-use and for applying green siltstone as potassium fertilizer.

ACKNOWLEDGMENTS

AUTHOR CONTRIBUTIONS

Conceptualization: (iD) João Carlos Ker (equal) and (iD) Luiz Aníbal da Silva Filho (equal).

Data curation: (iD) Danilo de Lima Camêlo (equal), (iD) David Lukas de Arruda Silva (equal), (iD) João Carlos Ker (equal), (iD) Luiz Aníbal da Silva Filho (equal), (iD) Marcelo Metri Corrêa (equal) and (iD) Maurício Paulo Ferreira Fontes (equal).

Formal analysis: (iD) João Carlos Ker (equal) and (iD) Luiz Aníbal da Silva Filho (equal).

Funding acquisition: (iD) João Carlos Ker (lead).

Investigation: (iD) João Carlos Ker (equal) and (iD) Luiz Aníbal da Silva Filho (equal).

Methodology: (iD) Danilo de Lima Camêlo (equal), (iD) David Lukas de Arruda Silva (equal), (iD) João Carlos Ker (equal), (iD) Luiz Aníbal da Silva Filho (equal), (iD) Marcelo Metri Corrêa (equal) and (iD) Maurício Paulo Ferreira Fontes (equal).

Project administration: (iD) João Carlos Ker (equal) and (iD) Luiz Aníbal da Silva Filho (equal).

Supervision: (iD) João Carlos Ker (lead).

Validation: (iD) Danilo de Lima Camêlo (equal), (iD) David Lukas de Arruda Silva (equal), (iD) João Carlos Ker (equal), (iD) Luiz Aníbal da Silva Filho (equal) and (iD) Marcelo Metri Corrêa (equal).

Writing – original draft: (iD) Luiz Aníbal da Silva Filho (lead).

Writing – review & editing: (iD) Danilo de Lima Camêlo (equal), (iD) David Lukas de Arruda Silva (equal), (iD) João Carlos Ker (equal), (iD) Luiz Aníbal da Silva Filho (equal), (iD) Marcelo Metri Corrêa (equal) and (iD) Maurício Paulo Ferreira Fontes (equal).

REFERENCES

Almeida Neto OB, Matos AT, Abrahão WAP, Costa LM, Duarte A. Influência da qualidade da água de irrigação na dispersão da argila de Latossolos. Rev Bras Cienc Solo. 2009;33:1571-81. https://doi.org/10.1590/S0100-06832009000600006

Alvares CA, Stape JL, Sentelhas PC, Gonçalves JLM, Sparovek G. Köppen's climate classification map for Brazil. Meteorol Z. 2013;22:711-28, https://doi.org/10.1127/0941-2948/2013/0507

Andrade GRP, Azevedo AC, Cuadros J, Souza Junior VS, Furquim SAC, Kiyohara PK, Vidal-Torrado P. Transformation of kaolinite into smectite and Fe-illite in Brazilian mangrove soils. Soil Sci Soc Am J. 2014;78:655-72. https://doi.org/10.2136/sssaj2013.09.0381

Andrade GRP, Cuadros J, Partiti CSM, Cohen R, Vidal-Torrado P. Sequential mineral transformation from kaolinite to Fe-illite in two Brazilian mangrove soils. Geoderma. 2018;309:84-99. https://doi.org/10.1016/j.geoderma.2017.08.042

Andrade GRP, Azevedo AC, Lepchak JK, Assis TC. Weathering of Permian sedimentary rocks and soil clay minerals transformations under subtropical climate, southern Brazil (Paraná State). Geoderma. 2019;336:31-48. https://doi.org/10.1016/j.geoderma.2018.08.026

Barbosa LCA, Fabris JD, Resende M, Coey JMD, Goulart AT, Cadogan J, Silva EG. Mineralogia e química de um Latossolo Câmbico desenvolvido de rocha pelítica do Grupo Bambuí, MG. Rev Bras Cienc Solo. 1991;15:259-66.

Chagas CS, Curi N, Duarte MN, Motta PEF, Lima JM. Orientação das camadas de rochas metapelíticas pobres na gênese de Latossolos sob Cerrado. Pesq Agropec Bras. 1997;32:539-48.

Clauer N, Keppens E, Stille P. Sr isotopic constraints on the process of glauconitization. Geology. 1992;20:133-6. https://doi.org/10.1130/0091-7613(1992)020<0133:SICOTP>2.3.CO;2

Conselho Estadual de Política Ambiental - Copam. Deliberação Normativa Copam nº 166, de 29 de junho de 2011: Altera o Anexo I da Deliberação Normativa Conjunta Copam CERH n° 2 de 6 de setembro de 2010, estabelecendo os Valores de Referência de Qualidade dos Solos. Belo Horizonte: Copam; 2011. Available from: http://www.siam.mg.gov.br/sla/download.pdf?idNorma=18414.

Corrêa MM, Ker JC, Mendonça ES, Ruiz HA, Bastos RS. Atributos físicos, químicos e mineralógicos de solos da região das Várzeas de Sousa (PB). Rev Bras Cienc Solo. 2003;27:311-24. https://doi.org/10.1590/S0100-06832003000200011

Deconinck JF, Strasser A, Debrabant P. Formation of illitic minerals at surface temperatures in Purbeckin sediments (Lower Berriasian, Swiss and French Jura). Clay Miner. 1988;23:91-103. https://doi.org/10.1180/claymin.1988.023.1.09

Donagemma GK, Ruiz HA, Fontes MPF, Ker JC, Schaefer CEGR. Dispersão de Latossolos em resposta à utilização de pré-tratamentos na análise textural. Rev Bras Cienc Solo. 2003;27:765-22. https://doi.org/10.1590/S0100-06832003000400021

Dooley JH. Baseline concentrations of arsenic, beryllium and associated elements in glauconite and glauconite soils in the New Jersey Coastal Plain. Trenton, NJ: New Jersey Geological Survey Investigation Report, New Jersey Department of Environmental Protection; 2001. https://doi.org/10.7282/T36M36B8

Furquim SAC, Barbiéro L, Graham RC, Queiroz Neto JP, Ferreira RPD, Furian S. Neoformation of micas in soils surrounding an alkaline-saline lake of Pantanal wetland, Brazil. Geoderma. 2010;158:331-42. https://doi.org/10.1016/j.geoderma.2010.05.015

Georgiadis A, Dietel J, Dohrmann R, Rennert T. What are the nature and formation conditions of hydroxy-interlayered minerals (HIMs) in soil? J Soil Sci Plant Nutr. 2020;183:12-26. https://doi.org/10.1002/jpln.201900283

Hammer Ø, Harper DAT, Ryan PD. PAST: Paleontological statistics software package for education and data analysis. Palaeontol Electron. 2001;4:4.

Harris W, White GN. X-ray diffraction techniques for soil mineral identification. In: Ulery AL, Drees LR, editors. Methods of soil analysis Part 5 - Mineralogical methods. Madison: American Society of Agronomy; 2008. p. 81-115. https://doi.org/10.2136/sssabookser5.5.c4

Huggett JM, Cuadros J. Glauconite formation in lacustrine/palaeosol sediments, Isle of Wight (Hampshire basin), UK. Clay Miner. 2010;45:35-49. https://doi.org/10.1180/claymin.2010.045.1.35

Jackson ML. Soil chemical analysis - advanced course: A manual of methods useful for instruction and research in soil chemistry, physical chemistry of soils, soil fertility, and soil genesis. 2nd ed. Madison: USA Department of Soil Science University of Wisconsin; 1979.

Jalali M, Meyari A. Heavy metal contentes, soil-to-plant transfer factors, and associated health risks in vegetables grown in western Iran. J Food Compos Anal. 2022;106:104316. https://doi.org/10.1016/j.jfca.2021.104316

Liguori BTP, Almeida MG, Rezende CE. Barium and its Importance as na indicator of (Paleo) productivity. An Acad Bras Cienc. 2016;88:2093-103. https://doi.org/10.1590/0001-3765201620140592

Lima ONB, Uhlein A, Britto W. Estratigrafia do Grupo Bambuí na Serra da Saudade e geologia do depósito fosfático de Cedro do Abaeté, Minas Gerais. Rev Bras Geocienc. 2007;37:204-15.

Maranhão DDC, Pereira MG, Collier LS, Anjos LHC, Azevedo AC, Cavassani RS. Genesis and classification of soil containing carbonates in a toposequence of the Bambuí Group. Rev Bras Cienc Solo. 2016;40:e0150295. https://doi.org/10.1590/18069657rbcs20150295

Maranhão DDC, Pereira MG, Collier LS, Anjos LHC, Azevedo AC, Cavassani RS. Pedogenesis in a karst Environment in the Cerrado biome, northern Brazil. Geoderma. 2020;365:114169. https://doi.org/10.1016/j.geoderma.2019.114169

McKeague JA, Day JH. Dithionite and oxalate - extractable Fe and Al as aids in differentiating various classes of soils. Can J Soil Sci. 1966;46:13-22. https://doi.org/10.4141/cjss66-003

Mehra OP, Jackson ML. Iron oxides removal from soils and clays by a dithionite-citrate bicarbonate system buffered with bicarbonate sodium. Clay Clay Miner. 1960;7:317-27.

Moreira DS, Uhlein A, Fernandes MLS, Mizusaki AM, Galéry R, Delbem ID. Estratigrafia, petrografia, e mineralização de potássio em siltitos verdes do Grupo Bambuí na região de São Gotardo, Minas Gerais. Geociências. 2016;35:157-71.

Moreira DS, Uhlein A, Dussin IA, Uhlein GJ, Misuzaki AMP. A Cambrian age for the Upper Bambuí Group, Brazil, supported by the first U-Pb dating of volvaniclastic bed. J South Am Earth Sci. 2020;99:102503. https://doi.org/10.1016/j.jsames.2020.102503

Moreira DS, Uhlein A, Uhlein GJ, Sial AN, Koester E. Ediacaran/Early Cambrian Serra da Saudade Formation, Bambuí Group: The sedimentary record of a foreland basin in Southeastern Brazil. Braz J Geol. 2021;51:e20210029. https://doi.org/10.1590/2317-4889202120210029

Mota JCA, Assis Júnior RN, Amaro Filho J, Romero RE, Mota FOB, Libardi PL. Atributos mineralógicas de três solos explorados com a cultura do melão na chapada do Apodi – RN. Rev Bras Cienc Solo. 2007;31:445-54. https://doi.org/10.1590/S0100-06832007000300004

Njuguna SM, Makokha VA, Yan X, Gitutu RW, Wang Q, Wang J. Health risk assessment by consumption of vegetables irrigated with reclaimed waste water: A case study in Thika (Kenya). J Environ Manage. 2019;231:576-81. https://doi.org/10.1016/j.jenvman.2018.10.088

Odom IE. Glauconite and celadonite minerals. Rev Mineral Geochem. 1984;13:545-84.

Oliveira CV, Ker JC, Fontes LEF, Curi N, Pinheiro JC. Química e mineralogia de solos derivados de rochas do Grupo Bambuí no norte de Minas Gerais. Rev Bras Cienc Solo. 1988;22:583-93. https://doi.org/10.1590/S0100-06831998000400003

Pereira TTC, Ker JC, Schaefer CEGR, Barros NF, Neves JCL, Almeida CC. Gênese de Latossolos e Cambissolos desenvolvidos de rochas pelíticas do Grupo Bambuí – Minas Gerais. Rev Bras Cienc Solo. 2010;34:1283-95. https://doi.org/10.1590/S0100-06832010000400026

Pinheiro Junior CR, Pereira MG, Azevedo AC, Huyssteen CV, Anjos LHC, Fontana A, Silva Neto EC, Vieira JN, Santos TG. Genesis and classification of carbonate soils in the State of Rio de Janeiro, Brazil. J S Am Earth Sci. 2021;108:103183. https://doi.org/10.1016/j.jsames.2021.103183

Ribeiro JF, Walter BMT. As principais fitofisionomias do Bioma Cerrado. In: Sano SM, Almeida SP, Ribeiro JF. Ecologia e flora. Brasília, DF: Embrapa; 2008. p. 152-212.

Rieder M, Cavazzini G, D'Yakonov YS, Frank-Kamenetskii VA, Gottardi G, Guggenheim S, Koval PV, Müller G, Neiva AMR, Rodoslovich EW, Robert JL, Sassi FP, Takeda H, Weiss Z, Wones DR. Nomenclatura of the micas. Can Mineral. 1998;36:905-12.

Ryan PC, Huertas FJ. The temporal evolution of pedogenic Fe-smectite to Fe-kaolin via interstratified haolin-smectite in moist tropical soil chronosequence. Geoderma. 2009;151:1-15. https://doi.org/10.1016/j.geoderma.2009.03.010

Santos RD, Lemos RC, Santos HG, Ker JC, Anjos LHC. Manual de descrição e coleta de solo no campo. 5. ed. rev. ampl. Viçosa, MG: Sociedade Brasileira de Ciência do Solo; 2015.

Santos HG, Jacomine PKT, Anjos LHC, Oliveira VA, Lumbreras JF, Coelho MR, Almeida JA, Araújo Filho JC, Oliveira JB, Cunha TJF. Sistema brasileiro de classificação de solos. 5. ed. rev. ampl. Brasília, DF: Embrapa; 2018.

Schwertmann U, Taylor RM. Iron oxides. In: Dixon JB, Weed SB, editors. Minerals in soil environments. Madison: Soil Science Society of America; 1989. p. 379-438.

Silva AA, Lana RMQ. Incubação do verdete com diferentes fontes de ácido para disponibilização de potássio, cálcio, magnésio do solo. Holos. 2015;5:73-83. https://doi.org/10.15628/holos.2015.3210

Silva AC, Vidal-Torrado P. Gênese dos Latossolos húmicos e sua relação com a evolução da paisagem numa área cratônicas do sul de Minas Gerais. Rev Bras Cienc Solo. 1999;23:329-41. https://doi.org/10.1590/S0100-06831999000200017

Silva LF, Fruett T, Zinn YL, Inda AV, Nascimento PC. Genesis, morphology and mineralogy of Planosols developed from different parent materials in Southern Brazil. Geoderma. 2019;341:46-58. https://doi.org/10.1016/j.geoderma.2018.12.010

Silva LG, Pufahl PK, James NP, Guimarães EM, Reis C. Sequence stratigraphy and paleoenvironmental significance of the Neoproterozoic Bambuí Group, Central Brazil. Precambrian Res. 2022;379:106710. https://doi.org/10.1016/j.precamres.2022.106710

Skiba M, Maj-Szeliga K, Szymanski W, Blachowski A. Weathering of glauconite in soils of temperate climate as exemplified by a Luvisol profile from Góra Puławska, Poland. Geoderma. 2014;235-236:212-26. https://doi.org/10.1016/j.geoderma.2014.07.013

Skoneczna M, Skiba M, Szymanski W, Kisiel M, Maj-Szeliga K, Blachowski A. Weathering of glauconite in alkaline soils of temperate climate: A case study from Górniki, eastern Poland. Geoderma. 2019;340:146-56. https://doi.org/10.1016/j.geoderma.2018.12.029

Soil Survey Staff. Keys to soil taxonomy. 12th ed. Washington, DC: United States Department of Agriculture, Natural Resources Conservation Service; 2014.

Tedrow JCF. Greensand and greensand soils of New Jersey: A review. New Brunswick: Departament of Ecology Evolution and Natural Resources, Rutgers University; 2002.

Teixeira PC, Donagemma GK, Fontana A, Teixeira WG. Manual de métodos de análise de solo. 3. ed. rev e ampl. Brasília, DF: Embrapa; 2017.

Teles LSB, Campos JEG, Ramos TG. Light on the origin of the verdetes siltstone, Bambuí group, central Minas Gerais State, Brazil. J S Am Earth Sci. 2022;119:103938. https://doi.org/10.1016/j.jsames.2022.103938

Uhlein GJ, Uhlein A, Pereira E, Caxito FA, Okubo J, Warren LV, Sial AN. Ediacaran paleoenvironmental changes recorded in the mixed carbonate-siliciclastic Bambuí Basin, Brazil. Palaeogeogr Palaeocl Palaeoecol. 2019;517:39-51. https://doi.org/10.1016/j.palaeo.2018.12.022

Vidal-Torrado P, Macias F, Calvo R, Carvalho SG, Silva AC. Gênese de solos derivados de rochas ultramáficas serpentinizadas no sudoeste de Minas Gerais. Rev Bras Cienc Solo. 2006;30:523-41. https://doi.org/10.1590/S0100-06832006000300013